ORIGINAL PAPER

Highly fluorinated poly(1,3,4-oxadiazole-ether)s. structural, optical and dielectric characteristics

**Alina-Mirela Ipate · Corneliu Hamciuc · Mihaela Homocianu ·
Valentina Elena Musteata · Alina Nicolescu · Maria Bruma · Nataliya Belomoina**

Abstract New fluorinated poly(1,3,4-oxadiazole-ether)s
were prepared by nucleophilic aromatic substitution technique
of an activated aromatic difluorinated compound with a
bisphenol containing three trifluoromethyl groups, namely 1,
1-bis(4′-hydroxyphenyl)-1-(3′,5′-ditrifluoromethylphenyl)-2,
2,2-trifluoroethane, **1**, or with a mixture of **1** and 9,9-bis(4-
hydroxyphenyl)fluorene. FTIR and NMR spectroscopy were
used to confirm the structure of the polymers. The polymers
were easily soluble in organic solvents and could be processed
in flexible thin films. The film surfaces exhibited hydrophobic
characteristics, as it was determined by contact angle measure-
ments. The polymers had high thermal stability, up to 440 °C,
and glass transition temperature in the range of 202–237 °C.
They showed fluorescence in the blue region, both in solution
and in solid state. The change in electronic absorption and
emission spectra of one of the polymer in neat and binary
solvent mixtures has been studied. Broadband dielectric spec-
troscopy was used to investigate the relaxation processes in
polymers. The dielectric constant of the polymers was in the
range of 2.84–2.96, at 100 °C and 10 kHz, and decreased with
the increase of fluorine content.

A.-M. Ipate (✉) · C. Hamciuc · M. Homocianu · V. E. Musteata ·
A. Nicolescu · M. Bruma
"Petru Poni" Institute of Macromolecular Chemistry, Aleea Grigore
Ghica Voda 41A, Iasi 700487, Romania
e-mail: ipate.alina@icmpp.ro

N. Belomoina
Nesmeyanov Institute of Organoelement Compounds, Vavilov St.
28, Moscow 119991, Russia

Introduction

Aromatic polyethers are a class of high performance
engineering thermoplastics having excellent mechanical
and thermal properties, chemical resistance and good
electroinsulating properties. The incorporation of 1,3,
4-oxadiazole rings into their macromolecular chains
improves the properties. Thus, aromatic poly(1,3,4-
oxadiazole-ether)s exhibit higher glass transition tem-
peratures and better thermal stability while maintaining
good hydrolitic stability, low dielectric constant, tough
mechanical behavior, and good solubility in common
organic solvents such as chloroform or tetrahydrofuran
[1–3]. Electron deficient 1,3,4-oxadiazole rings have
increased affinity to improve electron transporting
properties and therefore polymers containing this het-
erocycle are of great interest in the field of organic
light emitting diodes [4–6]. Also, the presence of a
free electron pair of nitrogen atoms in 1,3,4-oxadiazole
ring can facilitate the protonation that can modify the
optical properties [7].

In general, the presence of fluorine atoms in the unit struc-
ture of an aromatic polymer increases thermal stability, chem-
ical resistance and optical transparency and decreases the sur-
face energy, dielectric constant and water uptake [8, 9]. One
way to prepare aromatic fluorinated polymers is the incorpo-
ration of monomers containing trifluoromethyl (CF₃) groups.
These bulky groups do not allow a good packing of the mac-
romolecular chains thus increasing the free volume and im-
proving the solubility. The electronic polarizability of the
polymer decreases due to the low polarizability of the fluorine
atoms. The CF₃ groups can decrease the dielectric constant
due to the following effects: changes in the hydrophobicity,

changes in the free volume and in total polarizability. The free volume increases due to the relatively large volume of fluorine atom compared with hydrogen atom, which reduces the number of polarizable groups per volume unit, from which the dielectric constant of polymer decreases as the fluorine content increases [10–15].

An useful approach for reducing the melting temperature of the polymers and increasing solubility is the copolymerization of the monomers by which the symmetry of the structure is lowered and lateral packing is disrupted [3, 16]. The introduction of fluorene rings into the macromolecular chains of aromatic polymers improves the thermal stability, mechanical toughness and increases the glass-transition temperature. The polymers are soluble in different organic solvents and can be processed into flexible tough films. The presence of fluorene rings also improves the optical properties, the polymers exhibiting colorless light and high transparency. These polymers are interesting because of their applications as photoelectronic materials and gas separation membranes [16, 17].

In this article our effort was focused on the synthesis of specially designed new poly(1,3,4-oxadiazole-ether)s and the investigation of the relation between polymer structures and their thermal, optical and electrical properties. The CF_3 groups were introduced into the chemical structure of the polymers in order to obtain materials having lower dielectric constant and better solubility in a large number of solvents. The influence of CF_3 groups on polymer characteristics was discussed.

Experimental

Monomers

9,9-Bis(4-hydroxyphenyl)fluorene, **3**, was provided from Sigma Aldrich and used as received. N-methyl-2-pyrrolidone (NMP) was dried over phosphorus pentoxide and distilled under vacuum.

1,1-Bis(4′-hydroxyphenyl)-1-(3′,5′-ditrifluoromethylphenyl)-2,2,2-trifluoroethane, **1**, and 2,5-bis(p-fluorophenyl)-1,3,4-oxadiazole, **2**, were prepared according to published procedures [18, 19].
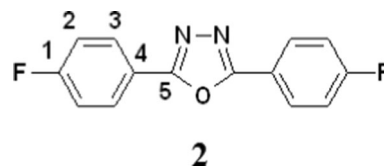

1
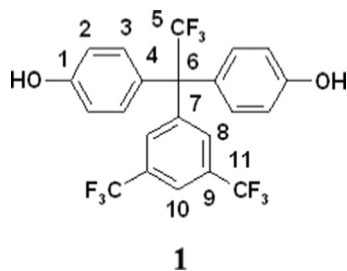
Monomer 1: FTIR (KBr pellets, cm^{-1}): 3320, 1615, 1516, 1370, 1280, 1130, 900, 832, 677.

^{1}H NMR (DMSO-d6) δ (ppm): 6.81 (4H, d, 9.2 Hz, H-2), 6.85 (4H, d, 9.2 Hz, H-3), 7.57 (2H, bs, H-8), 8.24 (1H, bs, H-10), 9.81 (2H, bs, OH).

^{13}C NMR (DMSO-d6), δ (ppm): 63.3 (1C, q, $^{2}J_{C-F}$=24 Hz, C-6), 115.5 (4C, C-2), 122.4 (1C, C-10), 122.9 (2C, q, $^{1}J_{C-F}$=274 Hz, C-11), 127.5 (1C, $^{1}J_{C-F}$=286 Hz, C-5), 128.2 (2C, C-4), 129.53 (2C, C-8), 130.4 (4C, C-3), 131 (1C, q, $^{2}J_{C-F}$=33 Hz, C-9), 143.5 (1C, C-7), 157.3 (2C, C-1).

^{19}F NMR (DMSO-d6), δ (ppm): -58.7 (F-5), -61.6 (F-11).

2

Monomer 2: FTIR (KBr pellets, cm^{-1}): 3070, 1625, 1590, 1550, 1490, 1470, 1240, 1030, 960.

**^{1}H NMR** (DMSO-d6), δ (ppm): 7.5 (4H, t, 8.8 Hz, H-2), 8.21 (4H, dd, 9.2 Hz, 5.6 Hz, H-3).

^{13}C NMR (DMSO-d6), δ (ppm): 116.6 (4C, d, $^{2}J_{C-F}$=22 Hz, C-2), 119.9 (2C, d, $^{4}J_{C-F}$=3 Hz, C-4), 129.4 (4C, d, $^{3}J_{C-F}$=9 Hz, C-3), 163.3 (2C, C-5), 164.1 (2C, d, $^{1}J_{C-F}$=250 Hz, C-1).

^{19}F NMR (DMSO-d6), δ (ppm): $-107.2 - -107.3$ (m, F-1)

Preparation of polymers **4**

The polymers **4** were prepared in a flask equipped with a nitrogen inlet, magnetical stirrer, Dean-Stark trap and condenser, according to a published procedure [3]. For the synthesis of **4a** the flask was charged with **1** (0.516 g, 0.002 mol), **2** (0.96 g, 0.002 mol), K$_2$CO$_3$ (0.604 g, 0.0043 mol), NMP (5.9 mL) and toluene (3.2 mL). The reaction mixture was heated at 140–150 °C for 5 h and water was removed by azeotropic distillation with toluene. The reaction was continued for 20 h at 170–180 °C and the resulted viscous polymerization mixture was cooled to room temperature, diluted with NMP (2 mL) and filtered to remove K$_2$CO$_3$. The solution was added dropwise into water, and the polymer was isolated, washed with methanol and boiling water, and vacuum dried. The copolymer **4b** was prepared by following the same procedure, from difluorinated compound **2** and equimolar amounts of bisphenols **1** and **3**.
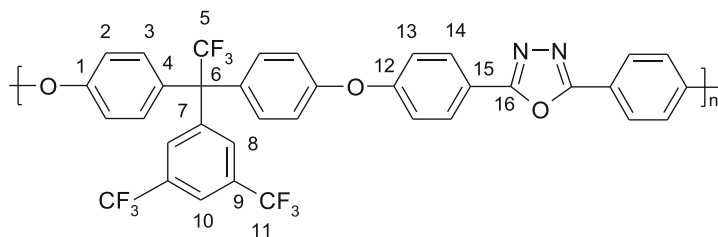
4a

Polymer 4a: Yield: 87 %.

FTIR (film, cm^{-1}): 3073, 1602, 1509, 1489, 1368, 1278, 1247, 1160, 1013, 961.

^{1}H NMR (CDCl$_3$) δ (ppm): 7.09 (4H, d, 8.6 Hz, H-2), 7.14 (4H, d, 8.7 Hz, H-3), 7.18 (4H, d, 8.3 Hz, H-13), 7.67 (2H, bs, H-8), 7.91 (1H, bs, H-10), 8.13 (4H, d, 8.2 Hz, H-14).

^{13}C NMR (CDCl$_3$), δ (ppm): 64.3 (1C, q, $^2J_{C-F}$=25 Hz, C-6), 119.2 (10C, C-2, C-13, C-15), 122.3 (1C, C-10), 123.0 (2C, q, $^1J_{C-F}$=273 Hz, C-11), 127.3 (1C, q, $^1J_{C-F}$=286 Hz, C-5), 128.9 (4C, C-14), 129.8 (2C, C-8), 131.4 (4C, C-3), 131.8 (2C, q, $^2J_{C-F}$=34 Hz, C-9), 133.9 (2C, C-4), 142.7 (1C, C-7), 156.3 (2C, C-1), 159.5 (2C, C-12), 164.0 (2C, C-16).

^{19}F NMR (CDCl$_3$), δ (ppm): −59.0 (F-5), −62.9 (F-11).
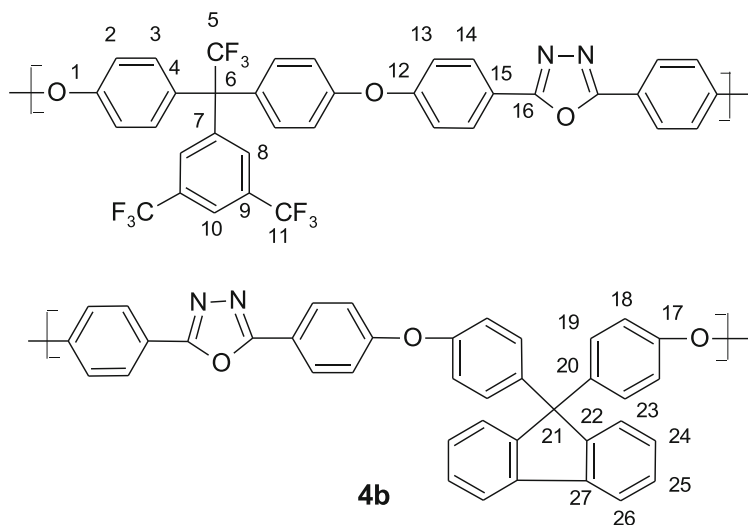
4b

Polymer 4b: Yield: 83 %.

FTIR (film, cm^{-1}): 3061, 1600, 1488, 1366, 1277, 1244, 1163, 1012, 984.

^{1}H NMR (CDCl$_3$) δ (ppm): 6.95 (4H, d, 7.20 Hz, H-18), 7.08–7.20 (16H, m, H-2, H-3, H-13), 7.24 (4H, d, 7.20 Hz, H-19), 7.32 (2H, t, 7.20 Hz, H-24), 7.40 (2H, t, 7.20 Hz, H-25), 7.45 (2H, d, 7.20 Hz, H-23), 7.68 (2H, bs, H-8), 7.80 (2H, d, 7.20 Hz, H-26), 8.04, 8.06, 8.11, 8.13 (8H, d, 7.20 Hz, 8.00 Hz, 7.60 Hz, 8.00 Hz, H-14, H-14', H-14", H-14''').

^{13}C NMR (CDCl$_3$), δ (ppm): 64.3 (1C, q, $^2J_{C-F}$=25 Hz, C-6), 64.5 (1C, C-21), 118.4 (4C, C-13), 119.2 (12C, C-2, C-13', C-15), 119.5 (4C, C-18), 120.3 (2C, C-26), 122.3 (1C, C-10), 123.0 (2C, q, $^1J_{C-F}$=274 Hz, C-11), 126.0 (2C, C-23), 128.3 (1C, q, $^1J_{C-F}$=287 Hz, C-5), 127.7 (2C, C-25), 127.9 (2C, C-24), 128.6, 128.7, 128.8, 128.9 (8C, C-14, C-14', C-14", C-14'''), 129.7 (4C, C-19), 129.8 (2C, C-8), 131.4 (4C, C-3), 131.8 (2C, q, $^2J_{C-F}$=34 Hz, C-9), 133.8 (2C, C-4), 140.0 (2C, C-27), 141.8, 141.9 (2C, C-20,

C-20'), 142.7 (1C, C-7), 150.9 (2C, C-22), 154.5 (2C, C-17), 156.2 (2C, C-1), 159.4, 159.5, 160.4, 160.5 (4C, C-12, C-12', C-12", C-12"'), 163.8, 163.9, 164.12 (4C, C-16, C-16', C-16", C-16"').

^{19}F NMR (CDCl$_3$), δ (ppm): −58.9 (F-5), −62.8 (F-11)

Preparation of polymer films

Films of polymers **4** were prepared by casting a solution of 5 % concentration of polymer in chloroform onto glass plates, followed by drying at room temperature for 24 h under a Petry dish and for another 5 h at 120 °C [20].

Measurements

The inherent viscosities (η_{inh}) of the polymers were determined with an Ubbelohde viscometer, by using polymer solutions in NMP, at a concentration of 0.5 g dL^{-1}, at 20 °C.

The molecular weight was determined by gel permeation chromatography (GPC) using UV and SLS detectors and PLgel 5μ Mixed C Agilent and PLgel 5μ Mixed D Agilent Columns. Measurements were carried out with polymer solutions in chloroform by using chloroform as eluent. Polystyrene standards of known molecular weight were used for calibration.

Fourier transform infrared (FTIR) spectra were recorded on FTIR Bruker Vertex 70 Spectrometer at frequencies ranging from 400 to 4000 cm^{-1}, by using KBr pellets or thin films having the thickness of 10–20 μm.

The NMR spectra were recorded on a Bruker DRX 400 spectrometer, equipped with a 5 mm multinuclear inverse detection probe, operating at 400.1, 100.6 and 376.4 MHz for ^{1}H, ^{13}C and ^{19}F nuclei, respectively. ^{1}H and ^{13}C chemical shifts are reported in δ units (ppm) relative to the residual peak of the solvent (ref. ^{1}H, CDCl$_3$: 7.26 ppm, DMSO: 2.51 ppm; ^{13}C, CDCl$_3$: 77.01 ppm, DMSO: 39.47 ppm). ^{19}F chemical shifts are electronically referred to CFCl$_3$ (0 ppm). H,H-COSY, H,C-HSQC, and H,C-HMBC experiments were recorded using standard pulse sequences in the version with z-gradients, as delivered by Bruker with TopSpin 1.3 PL10 operating software.

Microscopic investigations of the films were performed on an Environmental Scanning Electron Microscope (ESEM) type Quanta 200 operating at 30 kV with secondary and back-scattering electrons in high vacuum mode. Before analysis, the investigated films were covered with a thin layer of gold by sputtering (EMITECH K550X). The coupled dispersive X-ray spectroscope (EDX) permitted to perform the elemental analysis on the film surface.

Atomic force microscopy (AFM) images were taken in air, on a SPM SOLVER Pro-M instrument (from Russia). A NSG10/Au Silicon tip with a 35 nm radius of curvature and 255 kHz oscillation mean frequency was used. The apparatus was operated in semi-contact mode, over a 2×2 μm^2 scan area, 256×256 scan point size images being thus obtained.

The static contact angles were determined by the sessile drop technique using a CAM 101 contact angle meter (KSV Instruments) equipped with software for drop shape analysis. Measurements were carried out with water (W) and ethylene glycol (EG) as testing liquids. Contact angles were measured on 1 μL of wetting liquid, immediately after each droplet was added. The reported values are the average of six measurements from five droplets with separate locations.

Water vapors sorption capacity of the samples was measured by using the fully automated gravimetric analyzer IGAsorp supplied by Hiden Analytical, Warrington (UK). The vapors pressure was increased in 10 % humidity steps, each having a pre-established equilibrium time between 10 and 20 min. The cycle was ended by decreasing the vapor pressure in steps to obtain also the desorption isotherms. The drying of the samples before sorption measurements was carried out at 25 °C in flowing nitrogen (250 mL/min) until the weight of the sample was in equilibrium at RH below 1 %.

$$(\%) \text{ Water content} = \frac{W_{RH=82} - W_{RH=0}}{W_{RH=0}} \cdot 100 \qquad (1)$$

where $W_{RH=82}$ and $W_{RH=0}$ are weights of the sample at humidity value (RH)=82 % and of the sample completely dried, respectively. System measurements are fully automated and controlled by an user-friendly software package running on Microsoft® Windows™.

UV-Vis absorption and fluorescence spectra were recorded with a Shimadzu UV-3600 spectrophotometer and a Perkin-Elmer LS55 luminescence spectrometer, respectively. All solvents used in the present paper were spectrophotometric grade. For fluorescence measurements polymer films were prepared by using 1 % polymer solutions in CHCl$_3$, which were spin-coated on quartz slides at about 1000 rpm, for 30 s, at room temperature. Fluorescence emission spectra were registered at absorption maxima wavelength and for **4a** in DMF under excitation at 320, 330 and 340 nm. The binary mixtures were prepared by carefully mixing volumes of each solvent at room temperature. Each binary mixture was obtained in volume ratio of 1:5, 2:4, 3:3, 4:2 and 5:1.

Thermogravimetric analysis (TGA) was carried out in air, at a heating rate of 10 °C min^{-1}, using a Mettler Toledo TGA/SDTA 851^e balance. The heating scans were performed on 2 to 5 mg of sample in the temperature range 25–900°C. Alumina crucible (70 μl) is used as sample holder. The initial decomposition temperature is characterized as the temperature at which the sample achieves 5 % weight loss. The temperature of 10 % weight loss (T_{10}) and the temperature of maximum decomposition rate which is the maximum signal in differential thermogravimetry (DTG) curves were also recorded.

Differential scanning calorimetry (DSC) analysis was performed using a Mettler Toledo DSC 1 (Mettler Toledo, Switzerland) operating with version 9.1 of Stare software. The samples were encapsulated in aluminum pans having

pierced lids to allow escape of volatiles. The heating rate of 10 °C min^{-1} and nitrogen purge at 120 mL min^{-1} was employed. Heat flow versus temperature scans from the second heating run were plotted and used for reporting the glass transition temperature. The mid-point of the inflexion curve resulting from the typical second heating was assigned as the glass transition temperature (T_g) of the respective polymer.

The dielectric measurements were carried out using a Novocontrol Dielectric Spectrometer CONCEPT 40 (GmbH Germany). The samples were prepared in the form of films with thickness of 40–60 μm. The samples were sandwiched between two steel electrodes of diameter 20 mm and placed inside temperature controlled sample cell. Before dielectric measurements, the polymer films were heated in the dielectric setup at temperatures above T_g (to 250 °C), in order to remove any thermal history and to obtain good contact with the electrodes. Then, without removing the sample from the measuring cell, dielectric data expressed as complex permittivity (ε^*) given by Eq. (2):

$$\varepsilon^*(f) = \varepsilon'(f) - \varepsilon''(f) \qquad (2)$$

where ε' and ε'' are the relative permittivity and dielectric loss, respectively.

The dielectric data were collected at constant temperature as a function of frequency in 1 Hz to 1 MHz domain at every 5 °C between −120 °C and +250 °C. The amplitude of AC voltage applied between the electrodes was 1 V. The complex permittivity was converted to the complex dielectric modulus (M^*), according to Eq. (3):

$$M^*(f) = 1/\varepsilon^*(f) = M' + iM'' \qquad (3)$$

This formulation has the advantage of the suppression of high capacitance caused by space charge polarization phenomena [21].

Results and discussion

Synthetic procedure

Fluorinated poly(1,3,4-oxadiazole-ether)s 4 were prepared by nucleophilic aromatic substitution reaction of 2,5-bis(p-fluorophenyl)-1,3,4-oxadiazole, 2, with a bisphenol having a high fluorine content, 1, or with an equimolar amount of bisphenols 1 and 3, in the presence of K_2CO_3 (Scheme 1). The nucleophilic aromatic substitution of an aryl halide with a phenoxide is one of the most common routes to high performance aromatic polyethers. The oxadiazole moiety in monomer 2 can accept a negative charge and lower the activation energy for the displacement of p-substituted fluoro group through a Meisenheimer complex. For a thorough elimination of K_2CO_3 the polymer solutions were diluted and filtered.

Chemical structure and general characterization

The structures of the monomers 1 and 2 and polymers 4a and 4b were confirmed by FTIR and NMR spectroscopy. In FTIR spectra of the polymers characteristic absorption bands were observed at around 1247 cm^{-1} due to the presence of aromatic ether linkages and at 960 and 1013 cm^{-1} due to =C-O-C= stretching vibration in 1,3,4-oxadiazole ring. An absorption band situated at around 3070 cm^{-1} was due to aromatic C-H stretching vibration and the other two absorption bands appearing at 1600 and 1488 cm^{-1} were attributed to C=C stretching vibration of the aromatic groups. The strong absorption band at 1160 cm^{-1} was assigned to C-F stretching vibration in CF_3 groups.

In NMR spectra the assignments for the ^{1}H, ^{13}C and ^{19}F chemical shifts are based on 1D and 2D NMR homo- and heteronuclear correlations (H,H-COSY (Correlation Spectroscopy), H,C-HSQC (Heteronuclear Single Quantum Coherence) and H,C-HMBC (Heteronuclear Multiple Bond Coherence) and on ^{19}F-^{13}C couplings. The J-coupled protons were assigned from the H,H-COSY spectrum, while the carbons from CH groups were assigned from the H,C-HSQC

Scheme 1 Synthesis of fluorinated poly(1,3,4-oxadiazole-ether)s 4

4a: x = 1; y = 1; z = 0   4b: x = z = 0.5; y = 1
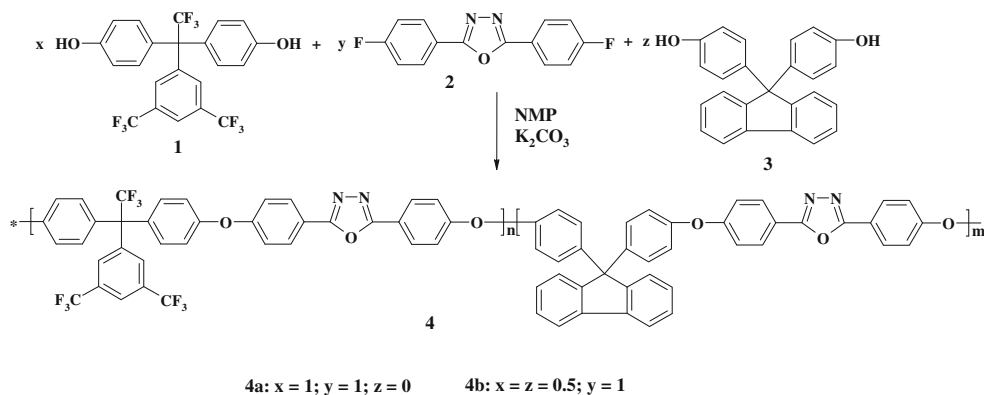
spectrum. The quaternary carbons were identified from the H, C-HMBC (Heteronuclear Multiple Bond Coherence) spectrum. The carbons situated in the vicinity of the fluorine nuclei were identified based on the characteristic ^{19}F-^{13}C couplings. The ^1H-, ^{13}C- and H,C-HSQC NMR spectra corresponding to **4a** are presented in Fig. 1. In ^1H NMR spectrum of **4a** (Fig. 1a) the protons *H-14* in *ortho* position to electron-withdrawing 1,3,4-oxadiazole ring appeared at the farthest

(a)

(b)

(c)

Fig. 1 ^1H NMR (**a**), ^{13}C NMR (**b**) and H,C-HSQC (**c**) spectra of **4a** in CDCl$_3$

downfield region of the spectrum. A shift to higher ppm values was observed for aromatic protons *H-8* and *H-10*, situated in *ortho* position to CF$_3$ groups. The protons *H-2* and *H-13* appeared at lower ppm values due to the electron donating properties of aromatic ether linkages. From the ^1H NMR spectra of **4b** it was found that the composition of the copolymer was closed to the composition of the reactants used for the synthesis. In the ^{13}C NMR spectrum of **4a** (Fig. 1b), all the carbon atoms resonated in the region 64.3–164.0 ppm, in which *C-5*, *C-6*, *C-9* and *C-11* showed clear quartet absorptions probably because of the $^2J_{C-F}$ and $^1J_{C-F}$ coupling atoms. As it can be observed the coupling effect decreased in the distance between C and F. For instance *C-5* and *C-11* showed a stronger C-F coupling effect than *C-6* and *C-9*. In ^{19}F NMR spectra of **4a** and **4b**, characteristic peaks for fluorine atoms of CF$_3$ groups, *F-5* and *F-11*, appeared at around −59.0 and −62.9 ppm, respectively.

The inherent viscosities of **4** were in the range of 0.192-0.207 dL g^{-1} (Table 1). The values of weight-average molecular weight (M_w) of **4a** and **4b** were 21, 700 and 14,300 g mol^{-1} and the number-average molecular weight (M_n) values were 79,000 and 38, 600 g mol^{-1}, respectively. Flexible thin films having the thickness in the range of 40–60 μm were prepared by casting the polymer solutions in chloroform (5 % concentration) and they were used for electrical measurements.

The solubility of **4** was tested in various organic solvents. The polymers were readily soluble in polar solvents like NMP, N,N-dimethylacetamide (DMAc), N,N-dimethylformamide (DMF), and even in less polar solvents like pyridine, chloroform and tetrahydrofuran. Their good solubility can be explained by a combination of factors: the presence in the unit structure of bulky CF$_3$ groups which increased the free volume, decreased the macromolecular interactions, thus improving the solubility; the presence of a large number of aromatic ether linkages which increased the flexibility of the macromolecular chains; in the case of **4b**, the presence of bulky fluorene groups and the copolymerization effect of two bisphenols (**1** and **3**) disturbed the packing of the polymer chains and contributed to create a distance between the macromolecular chains which facilitated the dispersion of small molecules of solvents between the polymer chains leading to better solubility. The excellent solubility makes the present fluorinated poly(1,3,4-oxadiazole ether)s potential candidates for practical applications in spin-coating and casting processes.

Very thin films with the thickness below 1 μm were prepared by spin-coating onto glass plates or onto
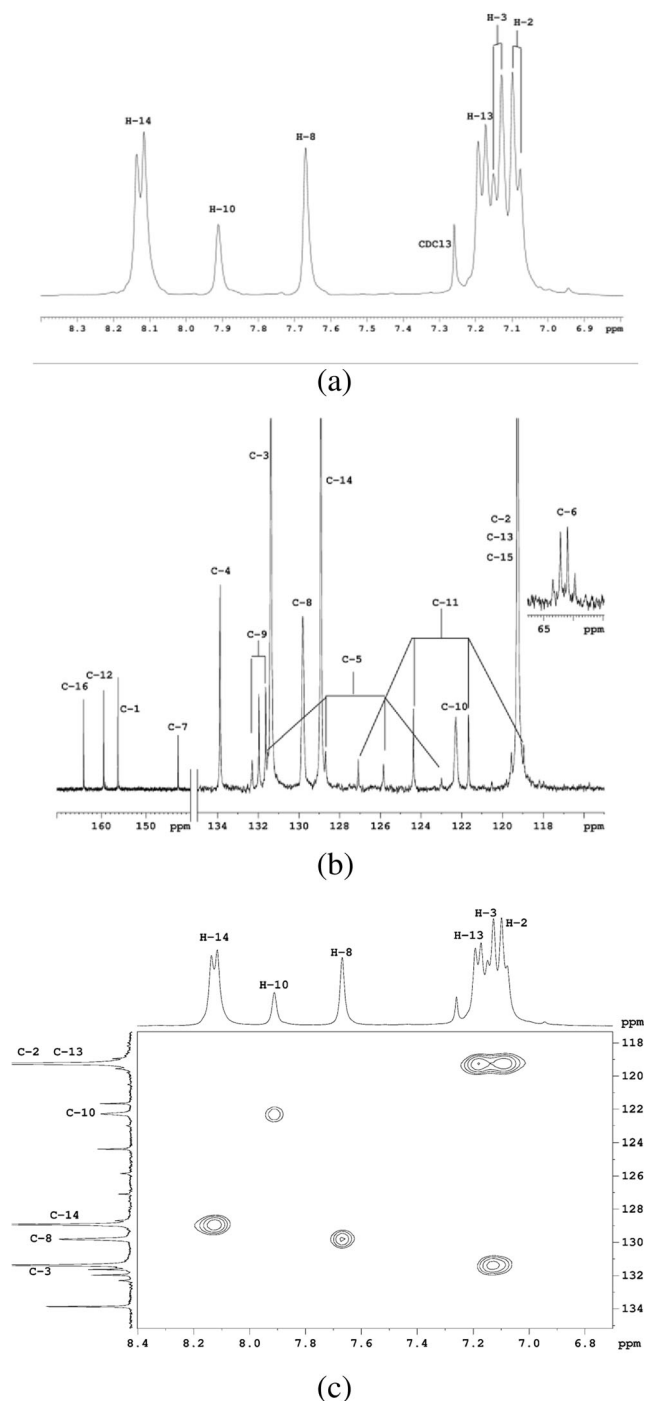
Table 1 The properties of polymers **4**

Polymer	η_{inh}[a] (dL g^{-1})	θ_W[b] (°)	θ_{EG}[c] (°)	γ_{sv}^{p} (mN m^{-1})	γ_{sv}^{d} (mN m^{-1})	γ_{sv} (mN m^{-1})	Weight change[d] (%)
4a	0.192	103.6±0.38	80.1±0.08	0.82	20.92	21.75	1.48
4b	0.207	94.3±0.20	68.1±0.50	2.80	22.68	25.49	3.78

[a] Inherent viscosity

[b] Contact angle with water

[c] Contact angle with ethylene glycol

[d] Total water adsorption at 25 °C and RH=82 %

silicon wafer by using very diluted polymer solutions (below 1 % concentration). The quality and the morphology of these films were studied by AFM. Figure 2 presents 2D and 3D AFM images of polymer film surface **4a**. As shown by AFM images the surfaces of the films were smooth and homogeneous, without cracks or pinholes, and presented various morphologies. The polymer films **4a** and **4b** exhibited the root mean square roughness (RMS) of 7–10 nm over 2×2 μm^2 area. The relatively high values of RMS may be attributed to the fact that CF$_3$ groups, more hydrophobic, were oriented to the air, a hydrophobic medium, while the less hydrophobic chains of the polymers were oriented to silicon wafer [22].

Contact angle, used as a measure of the wetting interaction between a liquid and a solid, represents the angle formed between a liquid and a solid surface when these materials are in contact. Wetting refers to the study of the ability of the liquids to form boundary surfaces with solid states. A wetting liquid is a liquid that forms a contact angle smaller than 90°, while non-wetting liquids create a contact angle between 90 and 180° with the solid. In the case of water, if the water contact angle is smaller than 90° the solid surface is considered hydrophilic, and if the water contact angle is larger than 90° the solid surface is considered hydrophobic.

Values obtained for contact angles with two liquids (water and ethylene glycol) for the polymer films **4** are presented in Table 1. In the case of water, as it can be seen from Table 1 and Fig. 3, the contact angle values were higher than 90° indicating that the films exhibited

Fig. 2 AFM images of aromatic polyeter **4a** film on silicon wafer: top view (**a**) and side view (**b**), section (**c**) and histogram (**d**)
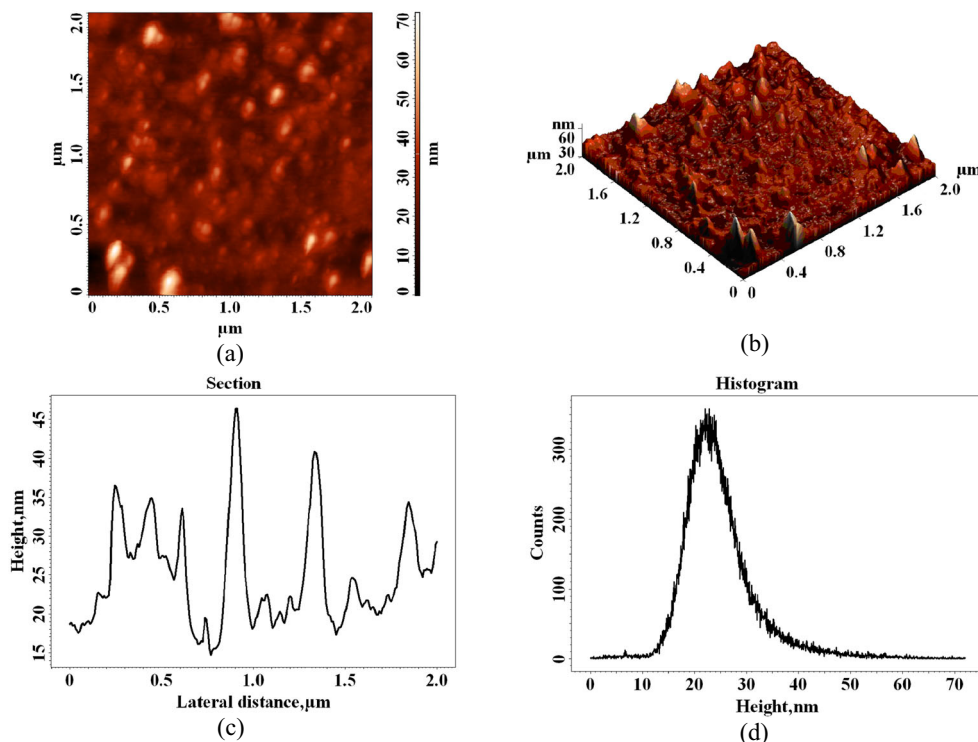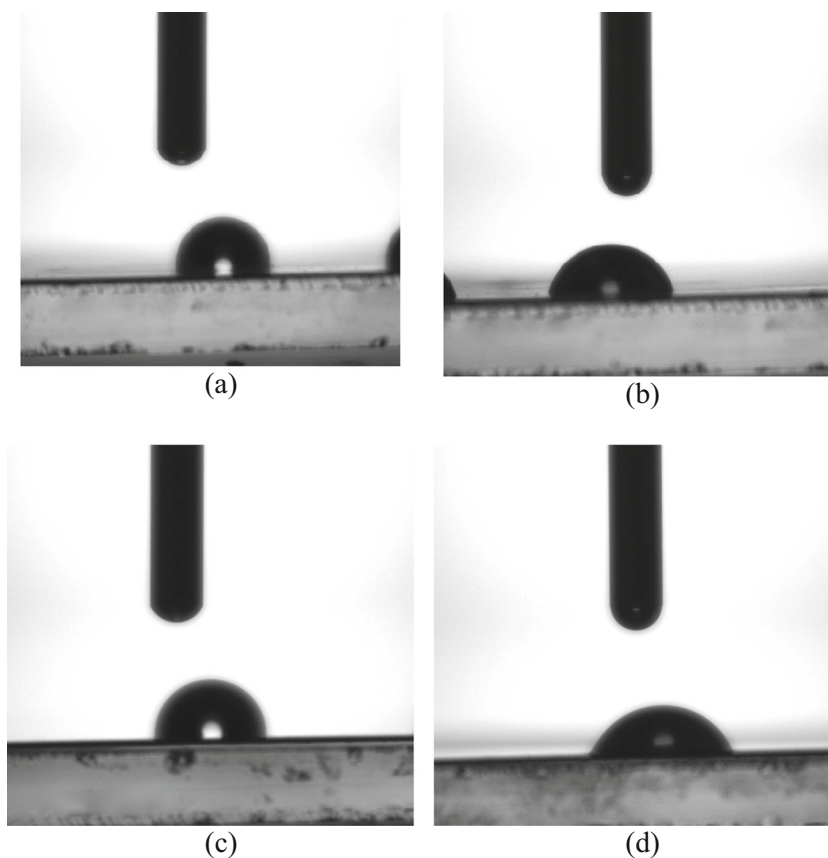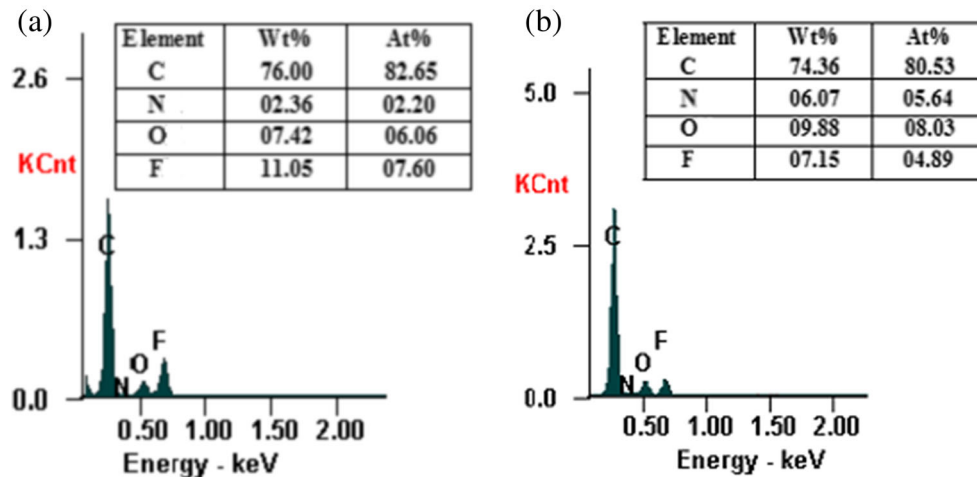
Fig. 3 Representative images of contact angles of the polymer films **4**: **4a** with water (**a**), ethylene glycol (**b**); **4b** with water (**c**), ethylene glycol (**d**)

(a)

(b)

(c)

(d)

good hydrophobicity. This can be explained by the presence of CF$_3$ groups in the chemical structure of the polymers, which led to an increase of hydrophobicity. The polymer **4a** having a higher concentration of fluorine atoms exhibited higher values for contact angle when compared with **4b** having a lower fluorine content. The concentration of fluorine atoms on film surfaces was evidenced by EDX measurements. The EDX method, able to identify the nature of the atoms present in the sample at a depth of 100–1000 nm from the surface, reveals the distribution of C, O, N and F atoms. As it can be observed from Fig. 4 the concentration of fluorine atoms on the film surface was much higher in the case of polymer film **4a** when compared with **4b**. In the case of ethylene glycol the contact angle exhibited lower values than 90° which suggest good wettability of polymer film surfaces.

Fig. 4 EDX results of polymers **4a** (**a**) and **4b** (**b**)

(a)

Element	Wt%	At%
C	76.00	82.65
N	02.36	02.20
O	07.42	06.06
F	11.05	07.60

(b)

Element	Wt%	At%
C	74.36	80.53
N	06.07	05.64
O	09.88	08.03
F	07.15	04.89

The surface properties of polymer films were studied by contact angle measurements. The surface free energy and its components were calculated using several equations.

The Young equation has the following form:

$$\gamma_{sv} = \gamma_{sl} + \gamma_{lv}\cos\theta \tag{4}$$

where γ_{sv} is the surface free energy at solid/vapor interface, γ_{sl} is the surface free energy at the solid/liquid interface, γ_{lv} is the liquid surface tension and θ is the contact angle between the solid and the measuring liquid. The values of γ_{lv} and θ can be easily measured but the quantity of γ_{sl} is unknown [23].

The orientation of the hydrophylic-hydrophobic groups at the film-air interface could be related to the polar (γ_{sv}^{p}) and dispersion factor (γ_{sv}^{d}) to the surface energy (γ_{sv}) [24]. The polar and dispersion components were calculated using the following equations Owens and Wendt [25]

$$\frac{1 + \cos\theta}{2} \cdot \frac{\gamma_{lv}}{\sqrt{\gamma_{lv}^{d}}} = \sqrt{\gamma_{sv}^{p}} \cdot \sqrt{\frac{\gamma_{lv}^{p}}{\gamma_{lv}^{d}}} + \sqrt{\gamma_{sv}^{d}} \tag{5}$$

$$\gamma_{sv} = \gamma_{sv}^{d} + \gamma_{sv}^{p} \tag{6}$$

where: γ_{lv} is liquid surface tension and γ_{sv} is the surface free energy at solid/vapor interface, the addition of d and p in the suprascripts refers to the dispersive and polar component, respectively. The Owens-Wendt approach is one of the most common methods for calculating the surface energy of polymeric materials.

By using the contact angles on the film surface with two liquids (water and ethylene glycol) the free surface energy components, γ_{sv}^{p} and γ_{sv}^{d}, were calculated by solving the resulting two-equation system. Average ($n=6$) contact angle values were considered to evaluate free surface energy. The surface tension and dispersive and polar components are for water (W) $\gamma_{lv}=72.8$ mN m^{-1}, $\gamma_{lv}^{d}=21.8$ mN m^{-1}, $\gamma_{lv}^{p}=51$ mN m^{-1} and for ethylene glycol (EG) $\gamma_{lv}=48$ mN m^{-1}, $\gamma_{lv}^{d}=29$ mN m^{-1}, $\gamma_{lv}^{p}=19$ mN m^{-1}. The surface tension γ_{sv} of **4a** ($\gamma_{sv}=21.75$ mN m^{-1}) was lower than the surface tension of poly(vinylidene fluoride) (PVDF) ($\gamma_{sv}=25$ mN m^{-1}), while surface tension γ_{sv} of **4b** ($\gamma_{sv}=25.49$ mN m^{-1}) was near to the surface tension of PVDF [26]. It can be observed an increase of γ_{sv}^{d} and γ_{sv}^{p} by reducing the fluorine content. Thus, the

copolymer **4b** having a lower concentration of fluorine showed higher values of γ_{sv}^{d} and γ_{sv}^{p}. In both cases the dispersive component is majority as compared with polar component. This permits to conclude that for the both investigated films the dipole forces and hydrogen-bond effects were very low. Also, the introduction of CF$_3$ groups reduced the surface tension and the film surface became more hydrophobic.

The work of adhesion for a liquid and a solid in contact, W_A, the work required to separate two surfaces from contact, can be expressed as Dupre's equation [23]

$$W_A = \gamma_{sv} + \gamma_{lv} - \gamma_{sl} \tag{7}$$

and from Young-Dupre's equation [27]

$$W_A = \gamma_{lv}(1 + \cos\theta) \tag{8}$$

The spreading coefficient, S_c, was determined from Dupré's equation [27]:

$$S_c = \gamma_{sv} - \gamma_{sl} - \gamma_{lv} \tag{9}$$

where γ_{sl} is

$$\gamma_{sl} = \gamma_{sv} + \gamma_{lv} - W_A \tag{10}$$

Girifalco and Good introduced the interaction parameter, Φ, between the surface and the liquid, defined as [27]:

$$\Phi = \frac{\gamma_{lv}(1 + \cos\theta)}{2(\gamma_{lv}\gamma_{sv})^{1/2}} \tag{11}$$

The values of work of adhesion, W_A, the spreading coefficient S_c and Girifalco-Good's interaction parameters for water (Φ(W)), and ethylene glycol (Φ(EG)) are listed in Table 2.

According to Young-Dupre's Eq. (8), W_A is dependent on the surface tension of the liquid and its contact angle on the substrate. Thus, the values for W_A increase when the contact angle decreases. As shown in Table 2, the magnitude of W_A, is higher for water than for ethylene glycol. The spreading coefficient values of the liquids used for contact angle measurements, calculated according to Eq. (9), are listed in Table 2. Generally, a positive value of S_c ($S_c > 0$), implies that the liquid

Table 2 Work of adhesion W_A, the spreading coefficient, S_c, the Girifalco-Good's interaction parameters Φ, for water (W) and ethylene glycol (EG)

Samples	W$_A$(W) (mN m^{-1})	W$_A$(EG) (mN m^{-1})	Sc(W) (mN m^{-1})	Sc(EG) (mN m^{-1})	Φ(W)	Φ(EG)
4a	55.68±0.45	56.25±0.065	−89.92±0.45	−39.75±0.075	0.69±0.05	0.86±0.005
4b	67.34±0.25	65.9±0.5	−78.26±0.25	−30.05±0.45	0.78±0.005	0.96±0.48

will spontaneously wet (complete wetting) and spread on a solid surface, whereas if it is negative ($S_c < 0$) partial wetting and spreading can be ascertained. It is seen that the values of the Sc for the polymer films were negative for the studied liquids. For water, S_c was more negative comparatively with S_c for ethylene glycol. These values indicate that ethylene glycol is better wetting agent when compared to water. This can be attributed to low surface tension and other properties of ethylene glycol (viscosity, density) [27].

For a good understanding of the degree of interaction between the test liquids and the film surfaces, the Girifalco-Good's interaction parameter Φ was calculated using Eq. (11); the obtained values for all studied samples are given in Table 2. Generally, a higher value indicates greater interaction and *vice versa* [27]. Φ (W) and Φ (EG), are the Girifalco-Good's interaction parameters due to water and ethylene glycol. It can be seen that the values of Φ for water were slightly lower when compared with those for ethylene glycol.

The process of water vapor sorption was used to study interaction between the adsorbed water and the surface of the film sample. Water adsorption of polymers heavily influences their dielectric constants and limits their applications in the electric and microelectronic industry. The sorption-desorption isotherms for **4a** and **4b** films are presented in Fig. 5. Maximum water vapor sorption values for the samples at 25 °C and RH = 82 % were in the range of 1.48–3.78 % (Table 1). According to IUPAC classification, the sorption-desorption curves can be associated to type IV curves. These types of isotherms describe sorption on hydrophobic/low hydrophilic material with weak sorbent-water interactions [28]. The low water vapor sorption of **4** was due to the presence of CF_3 groups which possess water repelling features thus decreasing the adsorption of moisture molecules on the surface of
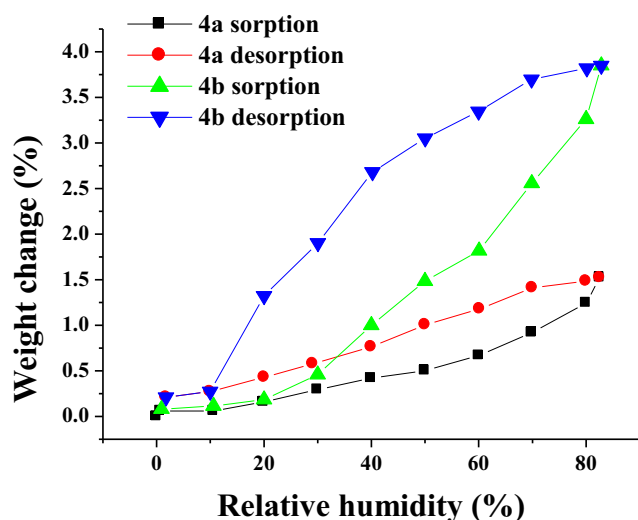
the fluorinated polymer films [29]. The polymer film **4a** exhibited lower water vapor sorption values (1.48 % at 82 % RH). This was due to the presence of a high content of fluorine atoms (26.58 wt%) which increased the hydrophobicity of the polymer. An increase of water vapor sorption appeared in the case of polymer film **4b** (3.78 % at RH = 82 %). In this case the fluorine content had lower value when compared to that of **4a** and as a consequence the hydrophobicity decreased leading to a higher value at 82 % RH.

Optical properties

The optical properties of the studied polymers were analyzed by UV-Vis and fluorescence spectroscopy. Absorption spectra of polymer solutions **4** are presented in Fig. 6a. These spectra showed a strong absorption maximum around 300 nm with one characteristic vibrational peak due to 2,5-diphenyl-1,3,4-oxadiazole unit [30].

The fluorescence spectra of **4a** solutions in chloroform and DMF are shown in Fig. 6b, and their corresponding spectral data are listed in Table 3. Both samples **4a** and **4b** showed a broad emission band located between 330–380 nm with two vibrational peaks (around 358 and 370 nm) and one a minor shoulder around 325 nm. Simultaneously, in Fig. 6b is present the fluorescence signal of **4a** in solid state, where we can investigate the influence of aggregating state on emission. In this spectrum a slightly red shift from that of polymer in solution was observed, indicating the presence of intermolecular interactions in solid state [31]. Moreover, the doublet observed in the spectra in solution became one broad band due to intermolecular interactions. Fluorescence spectra of **4b** have a pattern very similar to spectra for **4a** (Fig. 6c).

Figure 6d exhibits the emission spectra for **4a** recorded as a function of excitation wavelength (λ_{ex}) ranging from 300 to 340 nm. These spectra showed changes in the fluorescence intensity (decrease) due to excitation with different wavelengths, without changes in the shape and peak positions, which confirms the existence of a single emitting species.

Generally, the values of the Stokes shifts (SS) give the information concerning the differences between the absorbing ground state (S_0) and the emitting excited state (S_1). Moreover, the values are important to evaluate the performance of the investigated materials for use in organic light emitting diodes [32]. In our case, for the emission band with highest intensity ($\lambda_{em} = 358$ nm) moderate values for SS (58 nm, Table 3) were obtained, which indicate that the emitted light will be self-absorbed and implicitly the luminescence efficiency of the material will be slightly reduced. A not too small
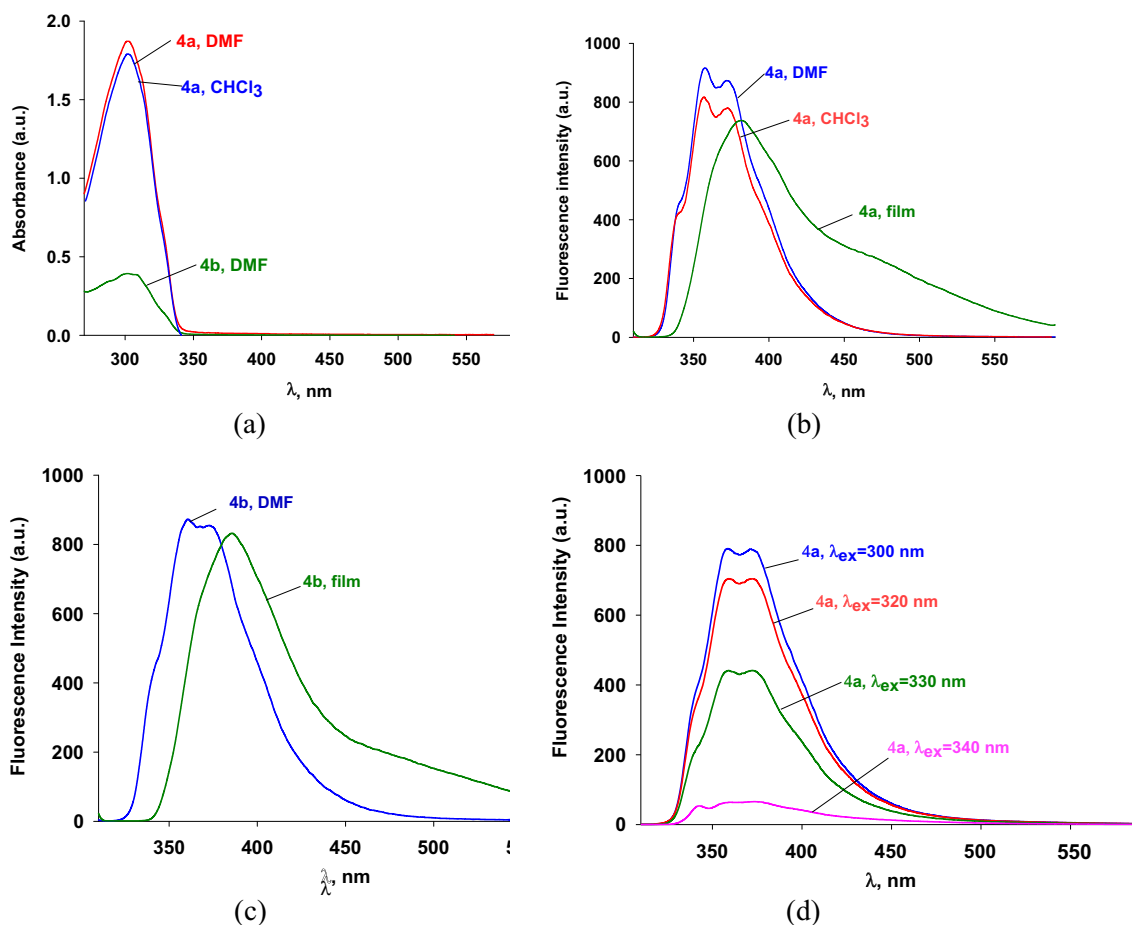
Fig. 5 The moisture sorption-desorption isotherms for polymers **4**

Fig. 6 Absorption (**a**) and fluorescence spectra of **4a** (**b**) and **4b** (**c**) in chloroform and DMF solutions and in solid state as film; fluorescence spectra of **4a** (**d**) in DMF under various excitation wavelengths

value for the Stokes Shift is confirmed by the existence of a little spectral overlap between the absorption and the emission bands. The Stokes shift values are quite similar for both compounds.

Table 3 Spectral properties of polymers **4**

Poly-mer	Solvents	Absorption			Fluorescence		
		$\lambda_{abs}{}^a$ (nm)	$\lambda_{edge}{}^b$ (nm)	$E_g{}^c$ (eV)	$\lambda_{ex}{}^d$ (nm)	$\lambda_{em}{}^e$ (nm)	Stokes shift (nm)
4a	DMF	301	365	3.40	300	358.5; 371	57.5; 70
					320	359; 372	58; 71
					330	359; 372	58; 71
	CHCl$_3$	302	360	3.45	300	357.5; 372	55.5; 70
	DMF+HCl	306	–	–	300	375	70
	film	–	–	–	300	385.5	–
4b	DMF	302	350	3.59	300	360.5; 372.5	58.5; 70.5
	film	–			300	382	–

[a] Wavelength of the maximum absorption

[b] The wavelength of the absorption edges of the optical absorption spectra

[c] Energy band gap

[d] Excitation wavelength

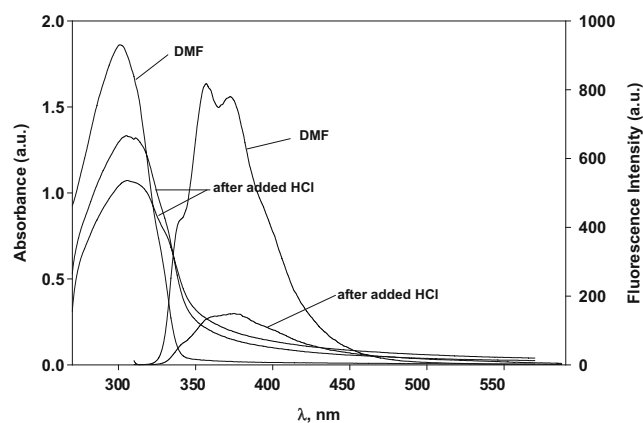[e] Wavelength of the maximum fluorescence

Fig. 7 UV-Vis and fluorescence spectra for unprotonated and protonated **4a** with HCl in DMF solution

The band gap energy, $E_g = h*c/\lambda_{edge}$, (h is Planck constant, c is speed of light and λ_{edge} is wavelength of the absorption edges of the optical absorption spectra) from absorption spectra of the studied polymers is listed in Table 3 and it was found very little varying with polymer structure.

The absorption and fluorescence spectra of **4a** in DMF solution, before and after protonation with HCl are shown in Fig. 7. It should be noted that the fluorescence intensity of the samples dramatically decreased with the added HCl, whereas the absorption intensity decreased slightly progressively upon HCl content increase. The absorption spectra of **4a** in presence of HCl were slightly red-shifted, suggesting that the samples environments were slightly altered (more polarity).

The absorption and emission characteristics of **4a** are sensitive to the type and quantities of solvents present in environmental media. The behavior of fluorinated polyoxadiazole **4a** was investigated in CHCl₃-DMF binary solvent mixture. Addition of different small amounts of DMF to the CHCl₃ solution of the polymer resulted in a slight red shift ($\Delta\lambda = 2$ nm) (Fig. 8) with simultaneous progressively absorption and fluorescence quenching. The observed quenching is attributed to hydrogen bonding formation with solvent molecules and solvent - solvent interactions [33]. The effect of changing solvent proportions in binary solvent mixtures
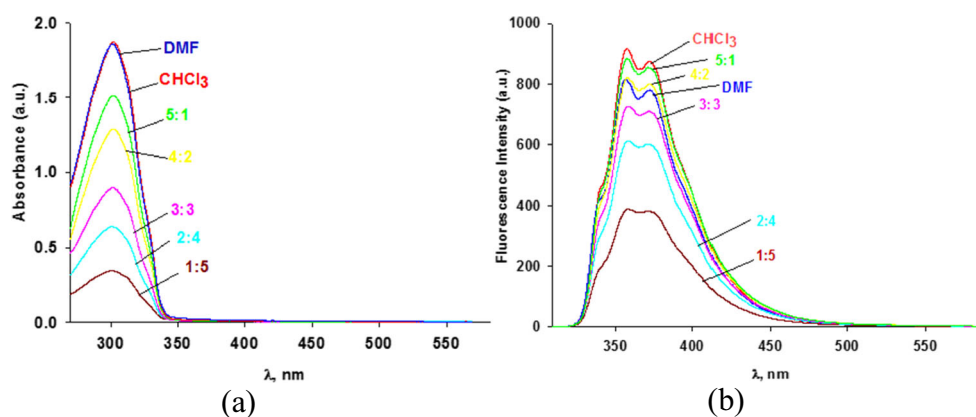
consisted in a prominent quenching without significantly affecting the profile of the absorption and emission spectra.

Thermal properties

The thermo-oxidative stability of polymers was evaluated by TGA measurements in air. The polymers exhibited high thermal stability. They began to decompose in the range of 447–459 °C, as indicated by the temperature of 5 % weight loss in TGA thermograms (Table 4). The temperature of 10 % weight loss was in the range of 487–492 °C. The degradation process exhibited one maximum of decomposition (T_{max}) in the range of 547–605 °C. An increase of T_{max} appeared in the case of **4b** ($T_{max} = 605$ °C) when compared with **4a** ($T_{max} = 547$ °C), due to the decrease of CF_3 group content and the presence of aromatic and bulky fluorene groups in polymer structure. The CF_3 groups can retard the free rotation even on their axis, resulting in a higher sterical and conformational energy that can be released by the loss of CF_3 groups, having as result the degradation during the heating process [29]. Also, at temperature higher than 500 °C the degradation of 1,3,4-oxadiazole rings with an increase of CN group content took place [34]. The data demonstrate that these polymers have high thermal stability similar to that of other poly(1,3,4-oxadiazole-ether)s without fluorine atoms in their chain [3].

The DSC measurements showed no evidence of crystalization or melting, suggesting that the polymers exhibited an amorphous morphology. The T_g values of the polymers, evaluated by DSC, were 202 and 237 °C for **4a** and **4b**, respectively. The T_g values were in concordance with the rigidity of the polymer backbone. Thus, the polymer **4a** exhibited a relatively low T_g value due to the presence of a high content of aromatic ether linkages which increased the flexibility of the macromolecular chains thus decreasing T_g. An increase of T_g of copolymer **4b** was observed due to the introduction of bulky fluorene groups into macromolecular chains which produced sterical hindrance and increased the rigidity of the macromolecules leading to higher T_g value.

Fig. 8 UV-Vis absorption (**a**) and fluorescence spectra (**b**) for **4a** in mixtures of CHCl₃ and DMF at different compositions, in volume (1:5- represent 1 mL CHCl₃ and 5 mL DMF)

(a)

(b)

Table 4 Thermal properties of polymers **4**

Polymer	$T_g{}^a$ (°C)	$T_5{}^b$ (°C)	$T_{10}{}^c$ (°C)	$T_{max}{}^d$ (°C)
4a	202	459	487	547
4b	237	447	492	605

[a] Glass transition temperature

[b] Temperature of 5 % weight loss

[c] Temperature of 10 % weight loss

[d] Maximum polymer decomposition temperature

Dielectric properties

Figure 9 presents the dependence of dielectric constant (ε') and dielectric loss (ε'') versus temperature, at different frequencies. In the entire temperature range, ε' decreased with increasing frequency because the response of dipolar units varies with frequency. At very low and moderate temperatures, up to 180 °C, ε' increased very slowly with the increase of temperature and ε'' presented small amplitude relaxation peaks attributed to local mobility of different polymer groups. When temperature reached T_g, the dielectric constant presented a well defined step increase for both of the samples and ε'' showed relaxation peak for **4a**. At a temperature higher than 180 °C a sharp increase of both ε' and ε'' can be observed, especially for low frequency values, due to effects of increased mobility of charge carriers. As the temperature increased the polar groups could rotate more smoothly.

Table 5 illustrates the ε' and ε'' values at two selected frequencies, 1 Hz and 10 kHz, and three selected temperatures, 20, 100 and 180 °C. It can be noticed that the polymers exhibited low ε' values. Thus, the values of ε' at 1 Hz were in the range of 2.88–3.31 at 20 °C, 2.90–3.27 at 100 °C and 2.96–3.96 at 180 °C, while at 1 kHz the values were in the range of 2.83–2.89 at 20 °C, 2.84–2.96 at 100 °C and 2.85–3.18 at 180 °C. The low values of the dielectric constant could be attributed to the presence of a high concentration of CF_3 groups in the unit structure. These groups contributed to decrease the dielectric constant in several ways: they increased the free volume of the polymer and reduced the polarizability of the molecules and the moisture absorption. The copolymer **4b** exhibited also low values of the dielectric constant in spite of lower fluorine content. This can be explained by the fact that the introduction of bulky fluorene groups increased the free volume of the polymer thus reducing the dielectric constant.

From Fig. 9 and Table 5 it can be also observed that ε'' exhibited low values in the interval up to 180 °C, which make possible their utilization as dielectrics to relatively high temperatures. This indicates that the electrical signal loss will be lower in the dielectric medium due to minimal conversion of electrical energy into heat or to losses trough electrical conduction.
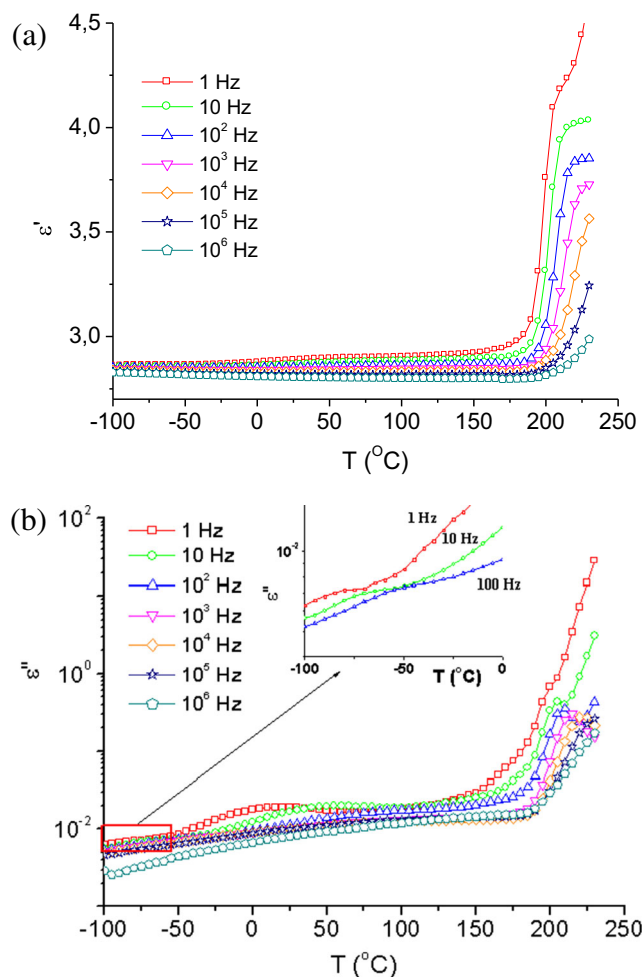

Fig. 9 Temperature dependence of dielectric constant (ε') (**a**) and dielectric loss (ε'') (**b**) at several frequencies for **4a**

In order to compare the relaxation behavior for the two polymers, the isothermally measured data were re-plotted in Fig. 10 as the variation of electrical modulus with temperature at several frequencies. Electric modulus $M^* = 1/\varepsilon^*$ representation is used to evidence electric field relaxation. The space charge effects at high temperatures are suppressed and a conductivity peak representing conductivity relaxation is revealed [35].

Variations of ε' and ε'' indicated dielectric activity in the measured temperature range. In negative temperature region, a weak γ relaxation was observed as a peak or a shoulder in ε'' representation for both polymers. For **4a** the process appeared as a small shoulder at −80 °C at 1Hz and shifted to higher temperatures with increasing frequency, so that, for frequencies higher than 10^3 Hz was overlapped by the next process. Compared to this polymer, the copolymer **4b** presented γ relaxation at much lower temperatures: at −115 °C for 10^4 Hz and for frequency $<10^4$ Hz it was at lower temperatures than the measurement interval ($< −120$ °C). At positive temperatures, the process was followed by other dipolar relaxation

Table 5 The dielectric constant and dielectric loss at different frequencies and temperatures

Polymer	Dielectric constant (ε')						Dielectric loss (ε'')					
	at 1 Hz			at 10 kHz			at 1 Hz			at 10 kHz		
	Temperature (°C)						Temperature (°C)					
	20	100	180	20	100	180	20	100	180	20	100	180
4a	2.88	2.90	2.96	2.83	2.84	2.85	0.019	0.018	0.087	0.009	0.013	0.014
4b	3.31	3.27	3.96	2.89	2.96	3.18	0.018	0.040	0.410	0.007	0.029	0.060

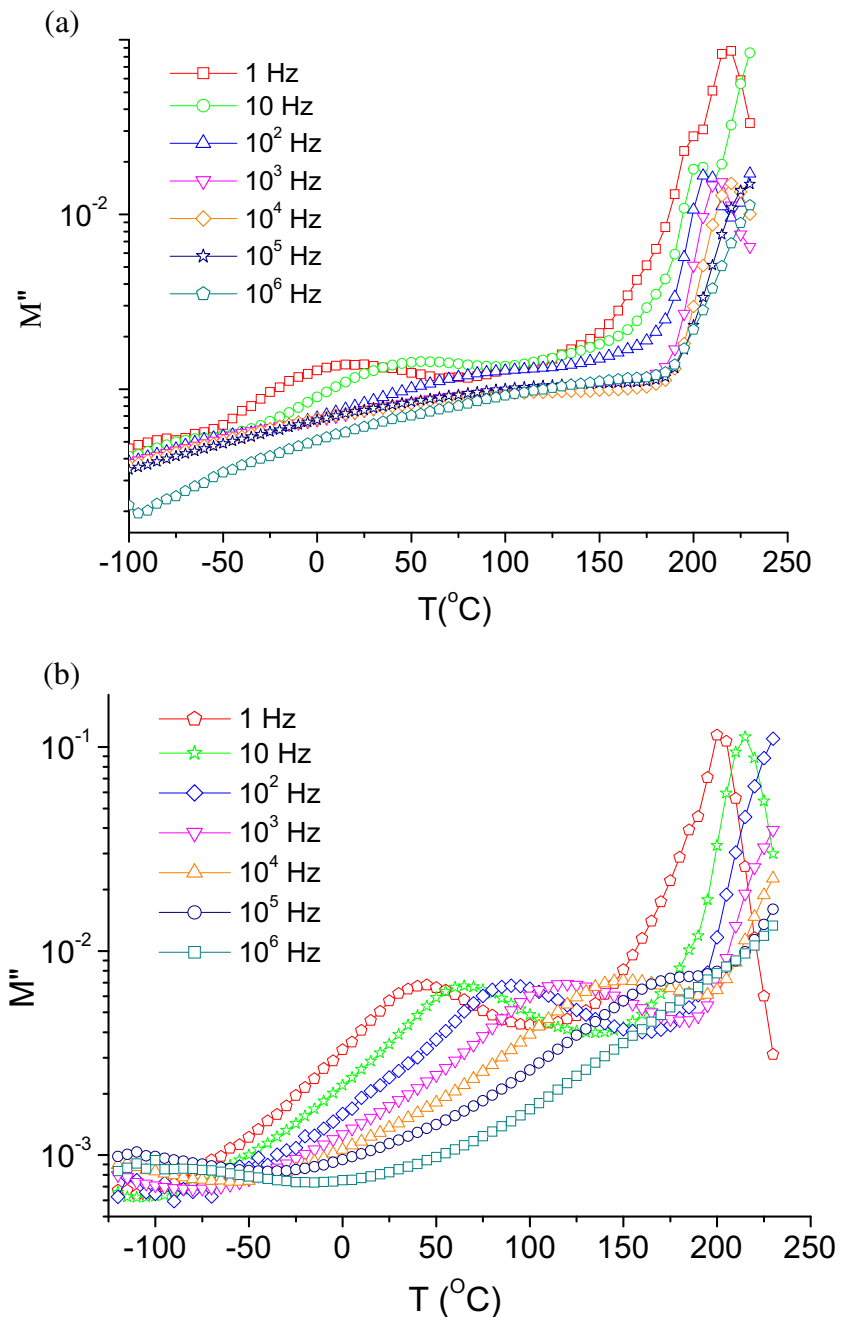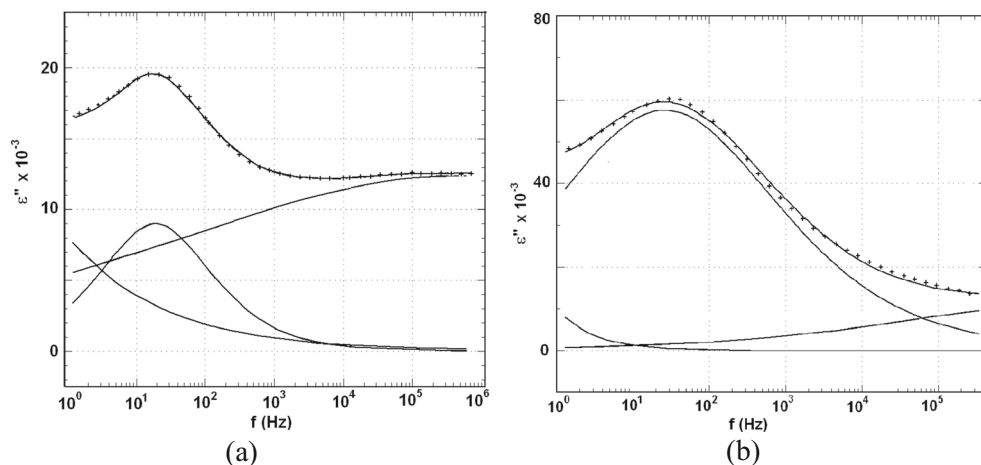**Fig. 10** Temperature dependence of dielectric modulus (M'') at several frequencies for **4a** (**a**) and **4b** (**b**)

Fig. 11 Fitting procedure for **4a**
(a) and **4b** (b) at 80 °C, in β
relaxation temperature range

(a)   (b)

observed as a peak in ε'' and M'' representations and step increase in ε' representation, generally designated as β relaxation. The two secondary relaxation processes occurring in glassy state were connected with local movements of polymer chain and the origin of the relaxations was not clear. Most probably γ relaxation is associated with phenyl ring local motions and is strongly influenced by moisture absorption, while for β relaxation it was found that may encompass larger portions of the repeating unit which respond in a correlated manner to the applied electric field [36, 37]. In more rigid systems, the origin of the β relaxation is linked to small amplitude motions that ultimately involve the entire repeat segment [38]. In this case the process could be assigned to cooperative conformational transitions involving nearby bonds that allow local conformational rearrangements without disturbing the overall trajectory of the chain [39, 40].

For our polymers, β relaxation appeared at 15 °C for **4a** and 45 °C for **4b** at 1Hz, suggesting reduced mobility for the copolymer with voluminous and rigid florene groups. On the high temperature side β relaxation was overlapped by other

Fig. 12 Arrhenius plot of *log τ* vs. 1000/T for β relaxation for **4b**

dipolar relaxation observed as a step increase with about two units of ε', which may be attributed to segmental relaxation associated to dynamic dielectric glass transition. This relaxation is better seen in dielectric permittivity representation for the middle frequencies, because at lower frequency was superimposed by a continuous steep increase associated with space charge polarization phenomena [41] and at the high frequency side was located at higher temperatures than the measured ones. For **4a**, α relaxation was also seen in ε'' representation as a shoulder for the lower frequencies due to overlapped conductivity losses and as peak at higher frequency. For **4b**, conductivity losses predominated in the ε'' representation at high temperatures. It is known that the increase of ε' and ε'' especially at low frequency is caused by increased mobility of the charge carriers that give rise to interfacial polarization and conductivity losses which mask other possible dipolar relaxations [42]. In addition, at these temperatures, the M'' dependence presented conductivity relaxation peaks indicating the formation of continuous network which permitted for the charge carriers to jump between neighboring localized sites in the entire volume of the polymer. For the polymer **4a** conductivity relaxation appears at 220 °C, while for the copolymer **4b** it appears at 200 °C, indicating higher mobility of charge carriers for **4b**.

In order to obtain more features of the relaxation processes, the frequency spectra are often fitted with characteristic functions which describe the dipolar relaxation peak, like Havriliak-Negami (HN) relation [43, 44]

$$\varepsilon^* = \varepsilon' - i\varepsilon'' = \varepsilon_u + \frac{\varepsilon_r - \varepsilon_u}{[1 + (i\omega\tau_{HN})^\alpha]^\beta} \quad (12)$$

where $\Delta\varepsilon = \varepsilon_r - \varepsilon_u$ represents the intensity of relaxation, ε_r and ε_u represent the relaxed ($\omega \rightarrow 0$) and unrelaxed ($\omega \rightarrow \infty$) values of the dielectric constant for each relaxation, $\omega = 2\pi f$ represents the angular frequency, f is the frequency, τ is the relaxation time for each process associated with peak maxima, and α and β represent the broadening and skewing parameters,
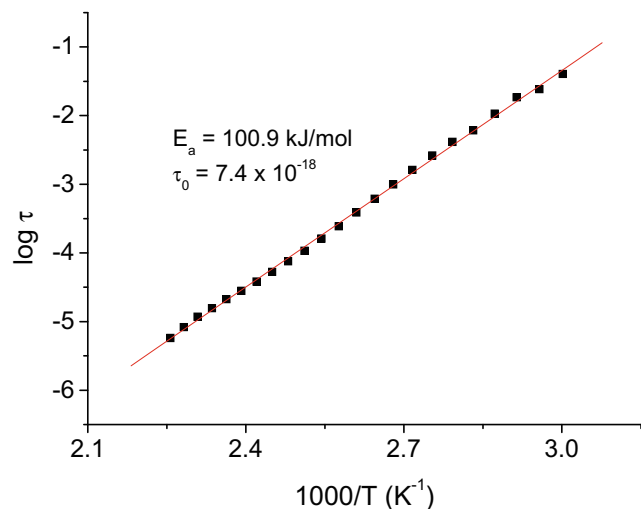
respectively. In our case, the frequency spectra for γ relaxation were very wide and had too small magnitude to be fitted with satisfactory accuracy. Also, they were overlapped with β relaxation at higher temperatures, especially for **4a**. The β relaxation spectra were fitted with a sum of two HN functions, for the two relaxation processes, as illustrated at 80 °C in Fig. 11. For conductivity contribution and other relaxation processes overlapping the relaxation peak in the low frequency side, an additional exponential term $(k\omega^{-n}, k$ - constant, n - exponential fitting parameter) was added.

The curve passing through the experimental points represents the sum of terms which describe conductivity losses at low frequency and the two HN terms, for β relaxation and for γ relaxation at high frequency. For **4a** β relaxation had a smaller intensity and was quite superimposed by conductivity at low frequency and a very wide γ relaxation, with a broadening parameter α less than 0.2, emerging from the measurement range at high frequency (Fig. 11a). Because of this, none of them can be described well by fitting. In the case of **4b** only a very small contribution for γ relaxation was observed (Fig. 11b).

The temperature dependence of the obtained relaxation times of β relaxation for **4b** was found to respect Arrhenius Eq. (13) (Fig. 12):

$$\tau(T) = \tau_0 \exp(E_a/kT) \tag{13}$$

where τ is the relaxation time associated with the peak maximum, E_a is the apparent activation energy of the process, k is Boltzmann's constant, τ_0 is the pre-exponential factor and represents the relaxation time at infinite temperature. From the slope of $log(\tau)=f(1/T)$ resulted a value of activation energy of 100.9 kJ/mol, which is comparable with other results reported in literature [3] for poly(1,3,4-oxadiazole-ether)s containing phthalide groups.

Conclusions

The introduction of CF_3 groups and fluorene moiety into the macromolecular chains of poly(1,3,4-oxadiazole-ether)s led to polymers with excellent solubility in organic solvents such as NMP, DMAc, DMF, chloroform and tetrahydrofuran. The polymer solutions in chloroform can be processed into flexible tough films having hydrophobic characteristics and low moisture uptake. The polymers were highly thermostable and showed high glass transition temperature. They exhibited fluorescence in the blue region when excited with UV light of 300–340 nm. The fluorescence properties were influenced by the nature of the solvent, excitation wavelength and protonation. A study of the influence of the DMF content in a mixture of DMF and CHCl₃ used as solvent for polymer **4a** showed that by increasing the DMF concentration a decrease

of fluorescence intensity appeared. Due to a high content of fluorine atoms these polymers exhibited low dielectric constant and low dielectric loss over a large interval of temperature and frequencies, which is very important for practical applications in microelectronics and related industries. The dielectric spectroscopy measurements evidenced the influence of trifluormethyl group content on the γ, β and α relation processes and conductivity relaxation process. It was evidenced that a higher content of trifluoromethyl groups lead to a temperature increase of conductivity relaxation process.

References

1. Hedrick JL, Twieg R (1992) Poly(aryl ether oxadiazoles). Macromolecules 25:2021–2025
2. Bottino FA, Di Pasquale G, Iannelli P (2001) Synthesis, characterization and study of the thermal properties of new poly(arylene ether 1,3,4-oxadiazole)s. Macromolecules 34:33–37
3. Hamciuc C, Hamciuc E, Ipate AM, Okrasa L (2008) Copoly(1,3,4-oxadiazole-ether)s containing phthalide groups and thin films made therefrom. Polymer 49:681–690
4. Sun YM (2001) Synthesis and optical properties of novel blue light-emitting polymers with electron affinitive oxadiazole. Polymer 42: 9495–9504
5. Chen Y, Huang YY, Wu TY (2002) Synthesis and characterization of luminescent polyethers with 2,5-distyrylthiophene and aromatic oxadiazole chromophores. J Polym Sci A Polym Chem 40:2927–2936
6. Yu YH, Chen Y (2003) Luminescent copoly(aryl ether)s containing of alternate oxadiazole and 1,4-distyrylbenzene derivatives: synthesis and characterization. J Polym Sci A Polym Chem 41:2765–2777
7. Grabiec E, Kurcok M, Schab-Balcerzak E (2009) Poly(amide imides) and poly(ether imides) containing 1,3,4-oxadiazole or pyridine rings: characterizations and optical properties. J Phys Chem A 113:1481–1488
8. Vora RH, Krishnan PSG, Goh SH, Chung TS (2001) Synthesis and properties of designed low-k fluoro-copolyetherimides. Part 1. Adv Funct Mater 11:361–373
9. Park SJ, Kim HS (2004) Influence of fluorination on surface and dielectric characteristics of polyimide thin film. J Colloid Interface Sci 272:384–390
10. Yang CP, Su YY (2003) Properties of organosoluble aromatic polyimides from 3′-trifluoromethyl-3,4′-oxydianiline. Polymer 44: 6311–6322
11. Yang CP, Hsiao SH, Wu KL (2003) Organosoluble and light-colored fluorinated polyimides derived from 2,3-bis(4-amino-2-trifluoromethylphenoxy)naphthalene and aromatic dianhydrides. Polymer 44:70967–7078
12. Zhu Z, Zhao P, Cai X, Meng WD, Qing FL (2004) Synthesis and characterization of novel fluorinated polyimides derived from bis[4-(4′-aminophenoxy)phenyl]-3,5-bis(trifluoromethyl)-phenyl phosphine oxide. Polymer 48:3116–3124
13. Yin D, Li Y, Yang H, Yang S, Liu J (2005) Synthesis and characterization of novel polyimides derived from 1,1-bis[4-(4′-

aminophenoxy)phenyl]-1-[3″,5″-bis(trifluoromethyl)phenyl]-2,2,2-trifluoroethane. Polymer 46:3119–3127

14. Li H, Liu J, Wang K, Fan L, Yang S (2006) Synthesis and characterization of novel fluorinated polyimides derived from 4,4′-[2,2,2-trifluoro-1-(3,5-ditrifluoromethylphenyl)ethylidene] diphthalic anhydride and aromatic diamines. Polymer 47:14443–1450

15. Jang W, Shin D, Choi S, Park S, Han H (2007) Effects of internal linkage groups of fluorinared diamine on the optical and dielectrical properties of polyimide thin films. Polymer 48:2130–21453

16. Hamciuc C, Hamciuc E, Ipate AM, Cristea M, Okrasa L (2009) Thermal and electrical properties of copoly(1,3,4-oxadiazole-ethers) containing fluorene groups. J Appl Polym Sci 113:383–391

17. Xu S, Yang M, Cao S (2006) A fluorescent copolyimide containing perylene, fluorene and oxadiazole units in the main chain. React Funct Polym 66:471–478

18. Tao L, Yang H, Liu J, Fan L, Yang S (2010) Synthesis of fluorinated polybenzoxazoles with low dielectric constants. J Polym Sci A Polym Chem 48:4668–4680

19. Hamciuc C, Hamciuc E, Bruma M (1996) Poly(1, 3, 4-oxadiazole-amide)s containing pendent phenoxy groups. High Perform Polym 8:507–514

20. Tullos GT, Cassidy PE, St. Clair AK (1991) Polymers derived from hexafluoroacetone: 12F poly(etherketone). Macromolecules 24:6059–6064

21. Macedo TB, Moynihan CT, Bose R (1972) The role of ionic diffusion in polarisation in vitreous ionic conductors. Phys Chem Glasses 13:171–179

22. Damaceanu MD, Constantin CP, Nicolescu A, Bruma M, Belomoina N, Begunov RS (2014) Highly transparent and hydrophobic fluorinated polyimide films with *ortho*-kink structure. Eur Polym J 50:200–213

23. Żenkiewicz M (2007) Methods for the calculation of surface free energy of solids. J Achiev Mater Manuf Eng 24:137–145

24. Srividhya M, Reddy BSR (2007) Synthesis and characterization of polyimide containing PEG/PDMS amphiphilic conetworks by hydrosilylation: Correlation between structure and properties. J Polym Sci A Polym Chem 45:1707–1726

25. Owens DK, Wendt RC (1969) Estimation of the surface free energy of polymers. J Appl Polym Sci 13:1741–1747

26. Bes L, Rousseau A, Boutevin B, Mercier R, Kerboua R (2011) Synthesis and properties of novel polyimides containing fluorinated alkoxy side groups. Macromol Chem Phys 202:2954–2961

27. Thomas SP, Thomas S, Abraham R, Bandyopadhyay S (2008) Polystyrene/ calcium phosphate nanocomposites: contact angle studies based on water and methylene iodide. Express Polym Lett 2:528–538

28. Sing KSW, Everett DH, Haul RAW, Moscou L, Pierotti RA, Rouquerol J, Siemieniewska T (1985) Reporting physisorption data for gas/solid systems with special reference to the determination of surface area and porosity. Pure Appl Chem 57:603–619

29. Li J, Zhang H, Liu F, Lai J, Qi H, You X (2013) A new series of fluorinated alicyclic-functionalized polyimides derived from natural-(D)-camphor: Synthesis, structure-properties relationships and dynamic dielectric analyses. Polymer 54:5673–5683

30. Xu SG, Yang MJ, Cao SK (2006) A fluorescent copolyimide containing perylene, fluorene and oxadiazole units in the main chain. React Funct Polym 66:471–478

31. Kim J, Levitsky IA, McQuade DT, Swager TM (2002) Structural control in thin layers of poly(p-phenyleneethynylene)s: photophysical studies of Langmuir and Langmuir-Blodgett films. J Am Chem Soc 124:7710–7718

32. Grucela-Zajac M, Filapek M, Skorka L, Gasiorowski J, Glowacki ED, Neugebauer H, Schab-Balcerzak E (2012) Thermal, optical, electrochemical, and electrochromic characteristics of novel polyimides bearing the acridine yellow moiety. Mater Chem Phys 137:221–234

33. Reichardt C, Welton T (2011) Solvents and solvent effects in organic chemistry, 4th edn. Wiley-VCH, Weinheim, Germany

34. Hamciuc C, Ipate AM, Hamciuc E, Lisa G (2008) Thermal degradation kinetics of some aromatic poly(1,3,4-oxadiazole-ether)s. High Perform Polym 20:296–310

35. Lee HT, Chuang KR, Chen SA, Wei PK, Hsu JH, Fann W (1995) Conductivity relaxation of 1-methyl-2-pyrrolidone-plasticized polyaniline film. Macromolecules 28:7645–7652

36. Sun Z, Dong L, Zhuang Y, Cao L, Ding M, Feng Z (1992) Beta relaxation in polyimides. Polymer 33:4728–4731

37. Habas JP, Peyrelasse J, Grenier-Loustalot MF (1996) Rheological study of a high-performance polyimide. Interpretation of the secondary mechanical relaxations of a nadimide crosslinked system. High Perform Polym 8:515–532

38. Ngai KL, Paluch M (2004) Classification of secondary relaxation in glass-formers based on dynamic properties. J Chem Phys 120:857–873

39. Bravard SP, Boyd RH (2003) Dielectric relaxation in amorphous poly(ethylene terephthalate) and poly(ethylene 2,6-naphthalene dicarboxylate) and their copolymers. Macromolecules 36:741–748

40. Comer AC, Kalika DS, Rowe BW, Freeman BD, Paul DR (2009) Dynamic relaxation characteristics of Matrimid® polyimide. Polymer 50:891–897

41. Chi Kao K (2004) Dielectric phenomena in solids. Elsevier Academic Press, San Diego

42. Kremer F, Schoenhals A (2003) Broadband dielectric spectroscopy. Springer Verlag, Berlin Heidelberg

43. Havriliak S, Negami S (1967) A complex plane representation of dielectric and mechanical relaxation processes in some polymers. Polymer 8:161–210

44. Havriliak S, Havriliak SJ (1997) Dielectric and mechanical relaxation in materials. Hanser, Cincinnati